PCCP

Accepted Manuscript

ROYAL SOCIETY OF CHEMISTRY

www.rsc.org/pccp

Journal Name

RSCPublishing

ARTICLE

X-ray absorption spectroscopy of tetrakis (phenyl)- and tetrakis(pentafluorophenyl)-porphyrin: an experimental and theoretical study

Cite this: DOI: 10.1039/x0xx00000x

Received 00th January 2012,
Accepted 00th January 2012

DOI: 10.1039/x0xx00000x

www.rsc.org/

Marco Vittorio Nardi,*[a,b] Roberto Verucchi,[b] Luca Pasquali,[c] Angelo Giglia,[d] Giovanna Fronzoni,[e] Mauro Sambi,[f] Giulia Mangione[f] and Maurizio Casarin*[f,g]

The unoccupied electronic structure of tetrakis(phenyl)- and tetrakis(pentafluorophenyl)-porphyrin thick films deposited on SiO_2/Si(100) native oxide surfaces has been thoroughly studied by combining the outcomes of near-edge X-ray absorption fine structure spectroscopy at the C, N, and F K-edges with those of scalar relativistic zeroth order regular approximation time-dependent density functional theory calculations carried out on isolated molecules. Both experimental and theoretical results concur to stress the electronic inertness of pristine porphyrin macrocycle based $1s^C \rightarrow \pi^*$ and $1s^N \rightarrow \pi^*$ transitions whose excitation energies are substantially unaffected upon fluorination. The obtained results complement those published by the same group about the occupied states of both molecules, thus providing the missing tile to get a thorough description of the halide decoration effects on the electronic structure of the tetrakis(phenyl)-porphyrin.

1. Introduction

Semiconductive properties of π-conjugated organic molecules are well known and widely probed for thick film electronic and opto-electronic devices by exploiting their p-type carrier transport. Among these systems, a great attention has been devoted to porphyrins and related derivatives as a consequence of their electronic and optical properties, which can be tuned and enhanced through molecular engineering.[1,2,3] In fact, the aromatic structure of these molecules makes them particularly appealing for use in electronics,[4] solar cells,[5] biological fields,[6] and sensing,[7] thus actually pushing towards the realization of a promising new generation of solid state devices. Moreover, the switch of electronic transport properties from p- to n-type through the substitution of hydrogen atoms on the outer molecular rim with halogen species such as fluorine is an intriguing opportunity, impelling research activity towards the study of organic systems having both electron acceptor and donor characteristics.[8] To this end, the investigation of the unoccupied electronic structure of tetrakis(phenyl)- and tetrakis (pentafluorophenyl)-porphyrin (hereafter, **I** and **II**, respectively) molecular films, complementing the one carried out by some of us on the occupied states of the same species, is herein reported.[8-9]

Thick films of **I** and **II** deposited on SiO_2/Si(100) native oxide surfaces by means of supersonic beams seeded by the organic precursor have been probed by using near-edge X-ray absorption fine structure (NEXAFS) spectroscopy to elucidate the nature, the localization and the relative energy positions of their low lying unoccupied molecular orbitals (MOs).[10] Actually, due to the highly localized character of core excitations, NEXAFS is solidly accepted as a site-sensitive probe of empty states. According to a well-established procedure,[8-9,11] NEXAFS spectra collected from thick films of both species have been rationalized with time-dependent density functional theory (TD-DFT) calculations[12-16] performed on isolated models. Although we are perfectly aware that the unoccupied electronic structure of **I** has been already studied both experimentally[17] and theoretically,[17b,18] we decided to revisit it to insure that theoretical results pertaining to **I** and **II** are homogeneous between them.

2. Experimental and computational details

NEXAFS experiments have been carried out at the BEAR end station (BL8.1L), at the left exit of the 8.1 bending magnet of the ELETTRA synchrotron facility in Trieste (Italy).[19] NEXAFS spectra have been collected in total electron yield (TEY) mode (*i.e.*, drain current mode) at the C, N, and F K-

edges, and normalized to the incident photon flux and to the clean substrate signal. Spectral energies have been calibrated by referring to the $4f_{7/2}^{Au}$ core level which has been obtained from an Au(100) sputtered sample (*i.e.*, carbon free). The synchrotron beam was elliptically polarized with the dominating components lying in the horizontal (*H*) plane, and the corresponding ellipticity, defined as $\varepsilon = \left|\vec{E}_V\right|^2 \times \left|\vec{E}_H\right|^{-2}$, equal to 0.1 (V stands for vertical plane and ε = 1 (0) for circularly (linearly) polarized light). Throughout the measurements, the incidence angle of the light with respect to the sample surface plane has been kept fixed at 10°. To correctly process the acquired data, each absorption spectrum has been first normalized to the drain current, which has been measured on an optical element (refocusing mirror) placed along the beam-line, and then normalized to the absorption spectrum attained under the same experimental conditions and energy range, on a Au(100) sputtered sample. The energy scale of each single spectrum has been re-calibrated taking into account the energy fluctuation of characteristic absorption features measured on the refocusing mirror.

Thick films of **I** and **II** (*i.e.*, 50 nm) have been grown in ultra high vacuum by supersonic molecular beam deposition in a preparation chamber (base pressure < 5×10^{-10} mbar) directly connected to the analysis chamber (base pressure < 1×10^{-10} mbar). The nominal film thickness (density, 2.2 g/cm^3) has been monitored by using a calibrated quartz crystal microbalance.

TD-DFT calculations have been carried out on **I** and **II** isolated species by using the Amsterdam Density Functional package.[12] The adopted geometrical parameters are those optimized in refs. 8 and 9 through the assumption of an idealized D_{2h} symmetry for both molecules. Ionization energies of N, C and F 1s-based MOs have been obtained by running scalar relativistic (SR) Zeroth Order Regular Approximation (ZORA) calculations,[20] and looking at the Kohn–Sham eigenvalues pertaining to the ground state (GS) electronic configuration. ZORA calculations have been run by adopting all-electron, triple-ζ with a polarization function, ZORA basis sets for all the atoms[21] and the LB94 approximate functional with the GS electronic configuration.[13,15] A further series of GS non-relativistic calculations have been run to get information about the lowest lying unoccupied frontier orbitals,[22] possible final MOs (*fmo*s) of NEXAFS transitions. The outcomes of these numerical experiments have been graphically displayed as density of states (DOS). In fact, these plots, based on the Mulliken's prescription for partitioning the overlap density,[23] afford an easy inspection of the atomic composition of MOs over a broad energy range. Partial DOS (PDOS) and DOS have been computed by using equations (1) and (2), respectively:[8-9,11]

$$PDOS_{n\ell}^{\nu}(\varepsilon) = \sum_p \frac{\gamma}{\pi} \frac{f_{n\ell,p}^{\nu}}{\left(\varepsilon - \varepsilon_p\right)^2 + \gamma^2} \qquad (1)$$

while

$$DOS(\varepsilon) = \sum_{\nu,n,\ell} PDOS_{n\ell}^{\nu}(\varepsilon) = \sum_p \frac{\gamma}{\pi} \frac{g_p}{\left(\varepsilon - \varepsilon_p\right)^2 + \gamma^2} \qquad (2)$$

where $f_{n\ell,p}^{\nu}$ is Mulliken's population contribution from the atom ν and the state $n\ell$ to the p^{th} MO of energy ε_p and degeneracy g_p. The Lorentzian broadening factor γ has been fixed equal to 0.25 eV. The Mulliken's prescription,[23] even though uniquely defined, is rather arbitrary; nevertheless, it yields at least a qualitative idea of the electronic localization. Moreover, 3D contour plots have been also employed to assign the σ* or π* character of selected MOs.

K-edge NEXAFS spectra of **I** and **II** have been simulated by evaluating excitation energies and corresponding oscillator strengths (*f*) for transitions having the $1s^{C/N/F}$-based MOs as initial MOs (*imo*s). To this end, SR-ZORA TD-DFT calculations[24] suitably tailored to treat core electron excitations have been run.[25] All electrons, quadruple-ζ with four sets of polarization functions, ZORA basis sets have been adopted for all the atoms;[21] moreover, two shells of diffuse functions, following the even tempered criterion, further augmented the basis sets of the F, N, and C atoms specifically involved in the excitations.[26] The adiabatic local density approximation[14] has been employed to approximate the XC kernel, while the LB94 approximate functional[15] with the GS electronic configuration has been adopted for the XC potential applied in the self consistent field calculations. Incidentally, Fronzoni *et al.*[13] have pointed out that, among approximate XC functionals having the correct asymptotic behaviour, a necessary condition for a proper description of high energy virtual orbitals and Rydberg states, the LB94 functional provides a satisfactory agreement between theory and experiment. Finally, scaled ZORA orbital energies[16] in the TD-DFT equations have been employed throughout to improve deep core excitation energies.

3. Results and discussion

I consists of the pristine porphyrin macrocycle (*pmc*) with four phenyl (Ph) rings bonded to the meso carbon atoms (C^5, C^{10}, C^{15}, and C^{20} in Fig. 1, where the recommended IUPAC 1–24 numbering system has been adopted) collectively tagged C^m.[27] Despite the bond delocalization (porphyrins are aromatic and they obey the Hückel's rule for aromaticity in that they possess $4n$ + 2 delocalized π electrons),[28] different chemical species may be identified in the molecule: (i) the pyrrolic nitrogen atoms, N^{21} and N^{23} (N^{PyH}), (ii) the iminic nitrogen atoms, N^{22} and N^{24} (N^{Py}); (iii) the twenty-four phenyl carbon atoms (C^{Ph}, chemically very similar); (iv) the four C^m atoms.

Different species of carbons may also be recognized in the non equivalent pyrrol rings; *i.e.*, those occupying the so called *α* (1, 4; 6, 9; 11, 14; 16, 19) and *β* (2, 3; 7, 8; 12, 13; 17, 18) positions, and, hereafter, collectively tagged C^{Py}. Besides those just mentioned, **II** includes a further atomic species (F) whose effects on the occupied electronic structure of **I** have been thoroughly discussed in ref. 8 (see PDOS and DOS reported in

Figs. 2 and 3; in Fig. 2 the $1s^C$ core level spectra of **I** and **II** have been also included for comparison).

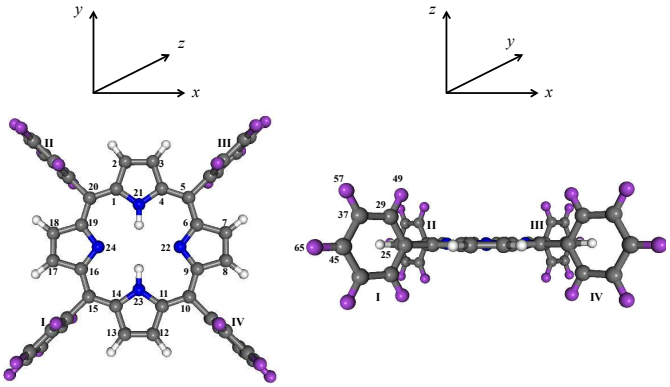

Fig. 1 Schematic representation (top and side view) of title molecules. Violet spheres correspond to H and F atoms in **H_2TPP (I)** and **H_2TPP(F) (II)**, respectively. The atom numbering corresponds to the one recommended by IUPAC and adopted by Nardi *et al.* in refs 8 and 9. In the selected framework, the pristine porphyrin macrocycle (*pmc)* lies in the *xy* plane and corresponds to the σ_h plane.

Among **I** and **II** heavy atoms (C, N and F), the *pmc* ones lie in the σ_h plane, while C^{Ph} and F species may be either parallel (||) or perpendicular ($\perp$) to it; C^{25}, C^{45}, F^{65} (C^{29}, C^{37}, F^{49}, F^{57}) and symmetry related atoms are then collectively tagged $C_{\parallel}^{Ph}$ and $F_{\parallel}$ ($C_{\perp}^{Ph}$ and $F_{\perp}$).

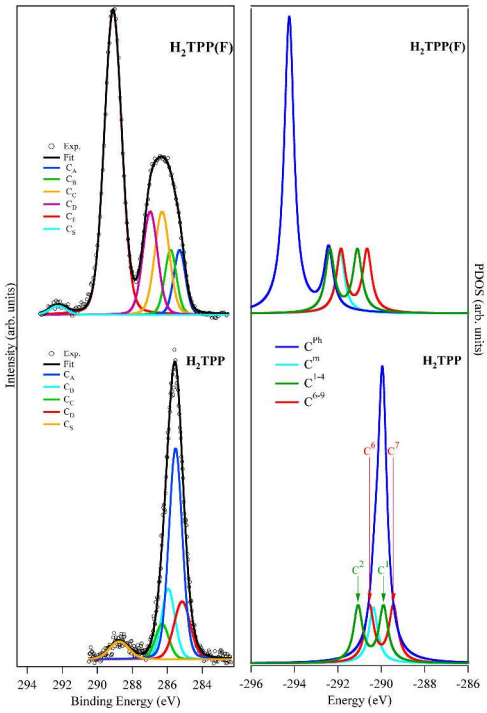

Fig. 2 (left panel) $1s^C$ core level spectra (background subtracted) from the **H_2TPP (I)** and **H_2TPP(F) (II)** films. The single components, shown in the legend, are related to the different carbon chemical species of the two molecules.[8-9] (right panel) SR-ZORA DFT **H_2TPP (I)** and **H_2TPP(F) (II)** $1s^C$ PDOS. Numerical labels adopted for both molecular species refer to the ones reported in Fig. 1.[8-9]

In the D_{2h} symmetry,[8-9] the linear combinations of 1s atomic orbitals (AOs) span the following irreducible representations (IRs): $a_g + b_{1g} + b_{2u} + b_{3u}$ (C^{Py}, C^m, $C_{\parallel}^{Ph}$, $F_{\parallel}$); $a_g + b_{1g} + b_{2g} + b_{3g} + a_u + b_{1u} + b_{2u} + b_{3u}$ ($C_{\perp}^{Ph}$ and $F_{\perp}$); $a_g + b_{2u}$ (N^{PyH}); $a_g + b_{3u}$ (N^{Py}).[29] Moreover, information about the localization of **I** and **II** unoccupied MOs, potential *fmo*s in X-ray absorption processes, may be gained by referring to Fig. 3 where contributions from heavy atoms 2p AOs to the DOS of **I** and **II** are displayed (lowest lying peaks associated to the empty levels are alphabetically labelled).

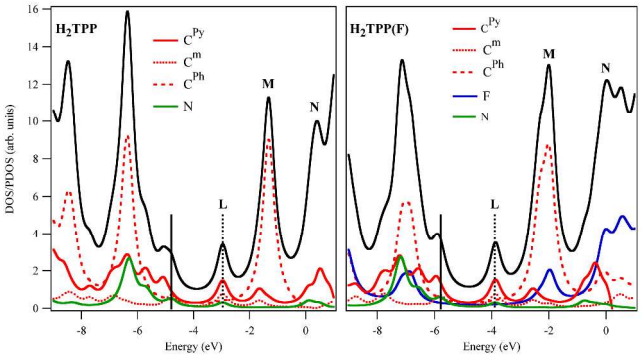

Fig. 3 **H_2TPP (I)** and **H_2TPP(F) (II)** DOS; contributions to the DOS coming from the heavy atoms 2p AOs are also included. Vertical bars represent the highest occupied MO (full line) and the lowest unoccupied MO (dotted line) energies.

The inspection of Fig. 3 clearly indicates that, both in **I** and **II**, the peak labelled as **L** is generated by 2p AOs of *pmc* atoms,[8-9] while major contributions to the higher lying features **M** and **N** come from C^{Ph} (**I**) and C^{Ph}/F (**II**) 2p AOs (**M**) and H 1s AOs (**N**). In more detail, two quasi degenerate $\pi_{\perp}$* MOs ($12b_{2g}/12b_{3g}$ in **I** and $21b_{2g}/21b_{3g}$ in **II**, see Fig. 4) contribute to **L**, while at least nine (thirteen) MOs participate to the generation of **M** in **I** (**II**).[30,32] Incidentally, among MOs generating **M**, only one $\pi_{\perp}$* orbital, namely the $11a_u$ MO in **I** (see Fig. 4) and the $20a_u$ MO in **II**, is present.

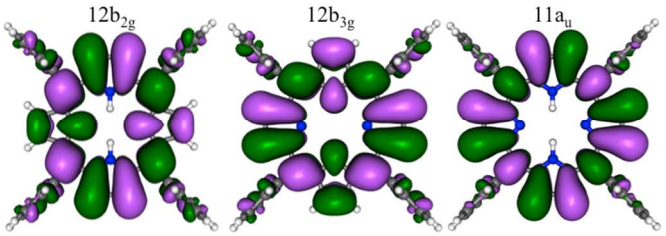

Fig. 4 3D plots of the **H_2TPP (I)** lowest lying unoccupied frontier orbitals. Displayed isosurfaces correspond to ± 0.02 $e^{1/2}Å^{-3/2}$ values. Corresponding MOs in **H_2TPP(F) (II)** ($21b_{2g}$, $21b_{3g}$ and $20a_u$) are indistinguishable from those depicted in the figure.

NEXAFS spectra. NEXAFS is unanimously recognized as an experimental tool able to provide a site-sensitive probe of the unoccupied electronic structure of molecules. Actually, since it implies the excitation of core electrons to unoccupied albeit bound valence orbitals as well as to shallow states in the near continuum, the localized character of core excitations makes K-edge spectra very sensitive to both the electronic structure and the local surroundings of the absorbing atom.

Extended NEXAFS spectra at the C, N and F K-edges of **I** and **II** thick films are displayed in Fig. 5, where main features have been identified and labelled with capital letters. Excitation energies taken into account range between 280 and 310 eV (C K-edge), 395 and 415 eV (N K-edge), 685 and 705 eV (F K-edge). According to literature,[11a,33-35] the ranges we considered have been split in two regions ([i] and [ii] in Fig. 5); the former is usually associated to $1s^C/1s^N/1s^F \rightarrow \pi^*$ excitations, whereas the latter accounts for $1s^C/1s^N/1s^F \rightarrow \sigma^*$ valence transitions. The inspection of Fig. 5, in particular of the C K-edge spectra, testifies the massive perturbation undergone by the electronic structure of **I** upon Ph fluorination. Symmetry, orbitals and spectra[31] have been cooperatively used to rationalize the effects of such a decoration.

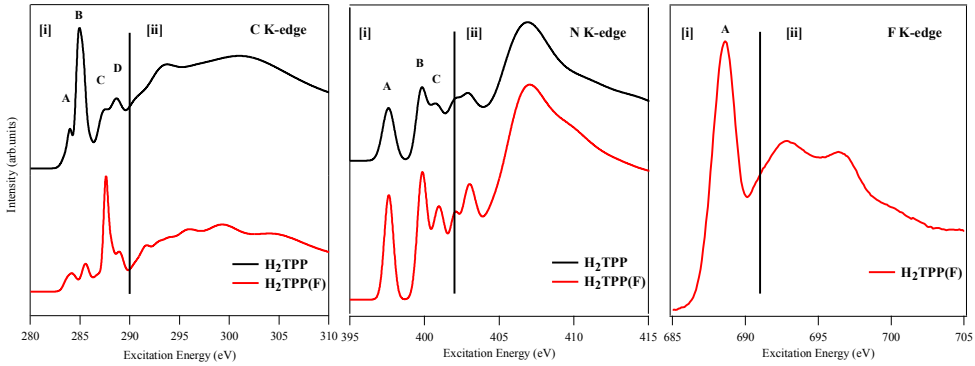

Fig. 5 Extended NEXAFS spectra of thick films of **H_2TPP (I)** (black line) and **H_2TPP(F) (II)** (red line) deposited on SiO_2/Si(100) native oxide surfaces. Vertical lines at 290 eV (left), 402 eV (middle) and 691 eV (right) separate [i] and [ii] regions (see text).

Now, before facing the assignment of NEXAFS spectra of **I** and **II**, it can be useful to spend a few words about title molecules spectroscopic differences foreseeable just on the basis of symmetry arguments. **I** and **II** electric dipole allowed transitions span the b_{1u}, b_{2u}, and b_{3u} IRs of the D_{2h} symmetry point group. In fact,

$$\Gamma_{GS} \otimes \Gamma_{\mu} \otimes \Gamma_{XS} \supset \Gamma_{a_g} \quad (3)$$

where Γ_{GS} is the electronic GS IR (a_g in the D_{2h} group), Γ_{μ} is the dipole moment operator IR (b_{1u}, b_{2u}, and b_{3u} in the D_{2h} group) and Γ_{XS} is the electronic excited state IR.[31] In the present case, electric dipole allowed transitions imply that

$$\Gamma_{\mu} = \Gamma_{XS} \quad (4)$$

with

$$\Gamma_{XS} = \Gamma_{imo} \otimes \Gamma_{fmo} \quad (5)$$

where, within the approximation, which reduces the complete one-electron excited configurations space (1h–1p space) to the subspace where only the core electrons are excited, Γ_{imo} and Γ_{fmo} are the IRs of the initial and final MOs, respectively.[36] As such, and before tackling experimental evidences, it can be useful to remind that, in the adopted geometry,[8-9] Ph rings are assumed to be perpendicular to σ_h (see Fig. 1); π^* orbitals are then $\perp$ ($\pi_\perp^*$) or $\parallel$ ($\pi_\parallel^*$) to σ_h according to their localization: $\perp$ if localized on the *pmc* atoms, $\parallel$ if localized on the C^{Ph} or F ones. Dipole allowed $1s \rightarrow \pi_\perp^*$ ($1s \rightarrow \pi_\parallel^*$) transitions will be therefore of b_{1u} (b_{2u} or b_{3u}) symmetry. Constraints for *imo*s and *fmo*s are summarized in Table 2-ESI.[31]

These considerations, simply based on symmetry arguments, point out that C-based $1s \rightarrow \pi^*$ excitations may be split in two sets, one including transitions of b_{1u} symmetry (hereafter, $\Pi_\perp$), the other including b_{2u} or b_{3u} transitions (hereafter, $\Pi_\parallel$). Focusing our attention on the former set, this can be further split in two subsets, one including transitions from ^{pmc}C 1s-based *imo*s (see Table 1-ESI; hereafter, $^{pmc}\Pi_\perp$), the other encompassing transitions from C^{Ph} 1s-based *imo*s (hereafter, $^{Ph}\Pi_\perp$). Since $^{pmc}\Pi_\perp$ transitions are completely localized on the *pmc*, they may be used as an internal gauge of the fluorination effects on the porphyrin electronic structure when moving from **I** to **II**.

C K-edge spectra. The [i] region of the C K-edge spectra of **I** and **II** is characterized by the presence of four main features, which cover an energy range of ~5 eV (see the fitted spectrum in Fig. 6);[37] moreover, a shoulder **S**, more evident in **II** than in **I**, is present on the lower energy side of the **A** band. In both spectra, the [i] region needed seven components, whose positions are reported in Table 1, to be properly fitted.

Table 1 Excitation energy position (eV) of C K-edge transitions (components a-d) for the fit of **H_2TPP (I)** and **H_2TPP(F) (II)** thick films spectra reported in Fig. 6. ΔE between similar features for **I** and **II** are also reported.

Component	**I**	ΔE	**II**	ΔE
a	283.72	-	283.53	-
a'	284.00	0.28	284.19	0.66
b	284.81	1.09	285.53	2.00
b'	285.28	1.56	-	
b"	285.78	2.06	-	
c'	-		286.90	3.37
c	287.30	3.58	287.57	4.04
c"	-		288.00	4.47
d	288.57	4.85	288.93	5.40

Before entering into the detail of the assignment of the C K-edge spectral features of **I** and **II** (see Tables 3-ESI and 4-ESI and Fig. 7), it may be useful to remind that Nardi *et al.* succeeded in identifying all carbon chemical species contributing to the complex C 1s spectrum of **II**.[9] In particular, the combined use of X-ray photoelectron spectroscopy and SR-

ZORA DFT calculations allowed some of us to state that the Ph rings fluorination results in a higher binding energy of the C^{Ph} 1s core levels, while the *pmc* C chemical species show less relevant differences when moving from **I** to **II** (see Fig. 2).

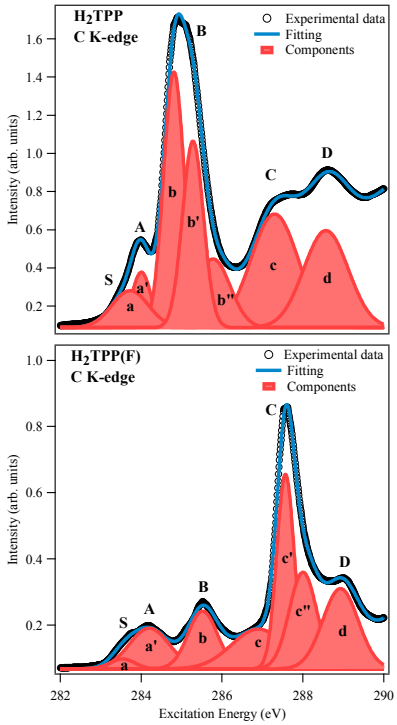

Fig. 6 Fitted [i] region of the C K-edge NEXAFS spectra of **H_2TPP (I)** (top) and **H_2TPP(F) (II)** (bottom).

A preliminary, sketchy assignment of the C K-edge spectra of **I** and **II** may be then attempted by exploiting the hypothesis that $^{pmc}\Pi_{\perp}$ transitions should have similar excitation energies in **I** and **II**, while the $\Pi_{\parallel}$ and, to a minor extent, the $^{Ph}\Pi_{\perp}$ ones should be blue shifted on passing from **I** to **II**. Accordingly, major contributions to the lowest lying band envelope **S** + **A** of both NEXAFS spectra should come from excitations (see Table 1-ESI, Fig. 2 and Fig. 3) associated to transitions from the b_{2u}/b_{3u} linear combinations of C^m-/C^{Py}-based 1s AOs to the lowest unoccupied MOs (LUMOs) of **I** ($12b_{2g}$ and $12b_{3g}$ MOs) and **II** ($21b_{2g}$ and $21b_{3g}$ MOs).

Relative intensity variations of bands **B** and **C** when moving from **I** to **II** ultimately state that the main contribution to the intensity of **B** in **I** and **C** in **II** has to be associated to $\Pi_{\parallel}$ and $^{Ph}\Pi_{\perp}$. Moreover, as far as the leftover band **B** in **II** and at least one component of **B** in **I** are concerned, they could be tentatively ascribed to a single excitation event corresponding to a transition having a b_{1g} linear combination of C^m-/C^{Py}-based 1s AOs as *imo*, and the $11a_u$ ($20a_u$) MO as *fmo* in **I** (**II**) (see Table 2-ESI and Fig. 4).[32] Besides these considerations, two further points need to be emphasized: i) the number of $1s^C$-based possible *imo*s is rather large and it corresponds to the number of C atoms present in the molecular skeleton (*i.e.*, 44, see Figure 1 and Table 1-ESI); ii) the energy range covered by the 44 linear combinations of the $1s^C$-based possible *imo*s is quite wide (1.6 and 3.6 eV in **I** and **II**, respectively, see Fig. 2). Highest lying NEXAFS features of the [i] region of both **I** and **II** might then include contributions not only from 1s → π* but also from 1s → σ* excitations, the former (latter) having the $1s^C$-based linear combinations with the highest (lowest) binding energies as *imo*s.

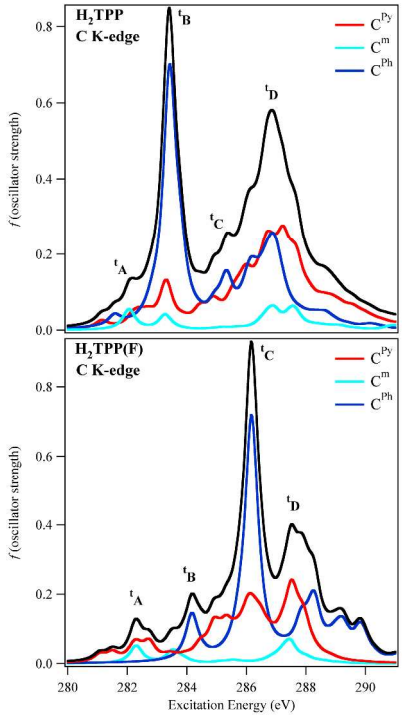

Fig. 7 SR-ZORA TD-DFT C 1s excitation spectra of **H_2TPP (I)** (top) and **H_2TPP(F) (II)** (bottom). Contributions from the different *imo*s are also displayed. Convoluted profiles have been obtained by using a Lorentzian broadening of 0.25 eV. SR-ZORA ionization limits may be deduced from the right panels of Fig. 2.[8-9,39]

Excitation energies and *f* values for the C 1s excitation spectrum of **I** and **II** as obtained from SR-ZORA TD-DFT[24] calculations are reported in Tables 3-ESI and 4-ESI, respectively, while the corresponding *f* distributions between 280 and 291 eV are displayed in Fig. 7.

The comparison between NEXAFS patterns and the $^{I}f^{C}/^{II}f^{C}$ distributions confirms the well-known excitation energy underestimation (in the present case ~2 eV), ultimately due to the XC potential deficiencies.[11,13b,25] Nevertheless, SR-ZORA TD-DFT outcomes prove that, even though the reference to the carbon PDOS of **I** and **II** (see Figs. 2 and 3) allows us to forecast the major contributions to the NEXAFS features, theoretical results are unavoidable to look into their details.

Starting with calculated data regarding **I**, the inspection of Table 3-ESI suggests that, according with our symmetry- and GS-based predictions (see Figs. 2 and 3), the **S** + **A** band envelope has to be associated to the seven lowest lying excitations, all of them corresponding to $\Pi_{\perp}$ transitions. More specifically, the $^{pmc}\Pi_{\perp}$ $10b_{2u}$ + $10b_{3u}$ → LUMOs[30] and the $^{Ph}\Pi_{\perp}$ $7b_{3u}$ → LUMO[30] transitions should contribute to **S**, while the remaining five excitations, all but one ($6b_{1g}$ → $11a_u$) corresponding to $^{pmc}\Pi_{\perp}$ transitions, should be hidden under the

A feature of Fig. 6 (top). Such an assignment perfectly agrees with that proposed by Di Santo *et al.*[17a] on a purely experimental ground, it concurs with theoretical results reported by Diller *et al.*[17b] and it sheds new light on the angle-dependent linear dichroism characterizing the NEXAFS C K-edge spectrum of a multilayer of **I**.[40] Nevertheless, it has to be remarked that the numerical agreement obtained by Diller *et al.*[17b] between theory and experiment is better than that we herein reported.

Even applying a quite severe filtering to the excitation selection (only those with ${}^{\mathbf{I}}f^{C} \geq 10 \times 10^{-3}$ have been included in Table 3-ESI), the analysis of theoretical outcomes states that, as preliminary foreseen, a really large number of excitations contributes to **B**, **C** and **D**.

This means that any detailed assignment of these features would simply be a matter of taste. Nevertheless, useful information can be obtained by looking into SR-ZORA TD-DFT results (see Fig. 7). The first thing to be noted is that the excitation energy range covered by the **I** [i] region (~5 eV, see Fig. 6 (top) and Table 1) is well reproduced by the ${}^{\mathbf{I}}f^{C}$ distribution reported in Fig. 7 (top). The same holds for the $\Delta E_{\mathbf{b'\text{-}b}}$ (0.47 eV, see Table 1), which is quantitatively reproduced by the range (0.54 eV, see Table 3-ESI) covered by the closely spaced excitations 8 – 19,[41] all but one ($6b_{1g} \rightarrow 11a_u$) associated to 1s → $\pi_{||}$* transitions having the linear combinations of Ph-based e_{2u} π* MOs as *fmos*.[40,42] The agreement of such an assignment with NEXAFS data of Di Santo *et al.*[17a] is twice as important because both the use of the isolated molecule approach to simulate NEXAFS features of a multilayer of weakly interacting molecules[8-9,11] and the assumption of a D_{2h} symmetry for **I**[9] are further reinforced.

In addition to the above considerations, the proposed assignment implies that the **b"** component of the NEXAFS spectrum of **I** has to be ascribed to a single excitation (the 20th in the Table 3-ESI) associated to the C^7-based $10b_{2u} + 10b_{3u} \rightarrow 14b_{3g} + 14b_{2g}$ transition. Incidentally, the energy difference (0.69 eV) between the 20th and the 19th excitation (see Table 1-ESI) agrees pretty well with the $\Delta E_{\mathbf{b''\text{-}b'}}$ (0.5 eV, see Table 1).

Moving to the broad and ill resolved bands **C** and **D** in Fig. 6, the only things that can be mined by theoretical outcomes and deserve to be mentioned are: i) C^m-based 1s AOs negligibly contribute to **C**; ii) C^{Py}- and C^{Ph}-based 1s AOs comparably contribute to **D**; iii) 1s → $\pi_{||}$* transitions associated to excitations hidden under **D** have the linear combinations of the Ph-based b_{2g} π* orbitals as *fmos*;[42] iv) more than 50% of the excitations reported in Table 3-ESI and associated to the feature **D** corresponds to 1s → σ* transitions. With specific reference to this last result, it has to be noted that, once again, it perfectly agrees with literature data.[17]

The striking differences characterizing the C K-edge NEXAFS spectra of **I** and **II** (see Fig. 6) have been already emphasized and, at a first look, they are quite well reproduced by the SR-ZORA TD-DFT ${}^{\mathbf{I}}f^{C}$ and ${}^{\mathbf{II}}f^{C}$ distributions. Moreover, the comparison of data reported in Table 3-ESI with those of Table 4-ESI indicates that ${}^{pmc}\Pi_{\perp}$ transitions, viable as internal gauge, can be straightforwardly identified in **II**.[43] Besides the very large blue shift of the $\Pi_{||}$ set upon the Ph rings fluorination,[44] a careful inspection of theoretical outcomes, including those that for space saving reasons are not included in the ESI, reveals that the lower excitation energy regions of **I** and **II** include the same number of transitions (seven) with $f \geq 10 \times 10^{-3}$. Nevertheless, their localization, intensities and composition are different. More specifically, the 2nd and 7th excitations of **I** (see Table 3-ESI), corresponding to transitions having as *imo*s the C^{29}-based 1s AOs, are strongly blue shifted upon the Ph ring fluorination[44] and substituted by the two C^2-based $12b_{3u} + 12b_{2u} \rightarrow 21b_{2g}^{(70)} + 21b_{3g}^{(30)}$ and $11b_{1g} \rightarrow 20a_u^{(99)}$ transitions, lying at 281.50 (${}^{\mathbf{II}}f^{C} = 18.646 \times 10^{-3}$) and 282.75 eV (${}^{\mathbf{II}}f^{C} = 18.838 \times 10^{-3}$) (see Table 4-ESI). Transitions reminiscent in **I** of those just described in **II** correspond to the C^2-based $8b_{3u} \rightarrow 12b_{2g}^{(100)}$ at 281.57 eV and $7b_{1g} \rightarrow 11a_u^{(100)}$ at 282.81 eV, not included in Table 3-ESI as a consequence of the adopted filtering (their ${}^{\mathbf{I}}f^{C}$ values are 0.49948×10^{-3} and 0.38949×10^{-3}, respectively). Such a result provides a first information, among many others (*vide infra*), about the effects induced by the F decoration of Ph rings on the *pmc* electronic properties: it may magnify the *f* values of excitations associated to specific transitions without significantly affecting their excitation energies.[45]

As far as the assignment of the NEXAFS features of **II** is concerned, SR-ZORA TD-DFT calculations induce us to assign all excitations hidden under the band envelope **S** + **A** and the lower excitation energy side of the leftover band **B** to transitions belonging to the ${}^{pmc}\Pi_{\perp}$ subset. In more detail, the shoulder **S** is ascribed to the lowest lying, C^7-based, $13b_{2u} \rightarrow 21b_{3g}$ transition, while the whole **A** feature is associated to the excitations 2 – 7 and the lower excitation energy side of the leftover band **B** to the ${}^{pmc}\Pi_{\perp}$ $9b_{1g} \rightarrow 20a_u$ transition. Interestingly, the whole band envelope **S** + **A** is substantially unaffected by the Ph rings fluorination. As a matter of fact, data reported in Table 1 indicate that, on passing from **I** to **II**, the **a′** component is slightly blue shifted (0.19 eV), while the **a** one is even red-shifted by the same amount. Both evidences are perfectly reproduced by SR-ZORA TD-DFT calculations, which ultimately establish the unresponsiveness upon fluorination of the selected internal gauge (compare in Table 3-ESI and Table 4-ESI the energies of the excitation selected as internal gauge).[43] Other excitations reasonably hidden under **B** are those (see Table 4-ESI) associated to 1s → $\boldsymbol{\pi}_{||}$* transitions localized on non-fluorinated $C_{||}^{Ph}$.

A comparison between components of bands **B** and **C** in **I** and **II**, similar to that considered for the band envelope **S** + **A**, is prevented by the substantial perturbation undergone by **B** and **C** upon fluorination; nevertheless, it is noteworthy that the above mentioned unresponsiveness of the ${}^{pmc}\Pi_{\perp}$ subset is systematically confirmed by comparing correlated transitions in the two molecules. A further example is provided by the comparison between the C^7-based $9b_{1g} \rightarrow 13a_u$ transition in **I** (excitation lying at 284.86 eV, see Table 3-ESI) and the C^7-based $12b_{1g} \rightarrow 23a_u$ transition in **II** (284.90 eV, see Table 4-ESI), both associated to the lower energy side of **C** in the corresponding NEXAFS spectra.[46] Moreover, even though the

excitations hidden under **C** with the highest *f* values correspond to $^{Ph}\Pi_{||}$ transitions localized on fluorinated C atoms and involving Ph-based e_{2u} $\pi_{||}$* orbitals, the contribution from excitations associated to 1s → $\pi_{\perp}$* and 1s → σ* transitions cannot be neglected (see Table 4-ESI). Differently to **I**, SR-ZORA TD-DFT outcomes indicate that no $^{Ph}\Pi_{||}$ transition having a linear combination of the Ph-based b_{2g} $\pi_{||}$* orbitals as *fmo* is present in the selected range (see Table 4-ESI).

As already mentioned, the inspection of Figs. 2 and 3 clearly shows that both core levels and the unoccupied electronic structure of **I** are considerably perturbed upon fluorination; nevertheless, the calculated blue shifts undergone by the core levels, in particular by the C^{Ph}-based 1s AOs, are significantly different with respect to the ones calculated for the unoccupied electronic structure.[47] Even though we are perfectly aware that different excitations imply different relaxation processes and that excitation energies cannot be directly compared with Kohn-Sham orbital energy differences, the similar blue shift undergone by $^{pmc}\pi_{\perp}$* and ^{pmc}C-based 1s AOs upon fluorination provides a rationale of the experimental unresponsiveness, theoretically confirmed, of the $^{pmc}\Pi_{\perp}$ subset.

N K-edge spectra. The [i] region of the N K-edge spectra of **I** and **II** is characterized by the presence of three main features, alphabetically labelled in Fig. 8, which cover an energy range of ~4 eV. These features have been fitted with three components whose excitation energy positions are reported in Table 2.

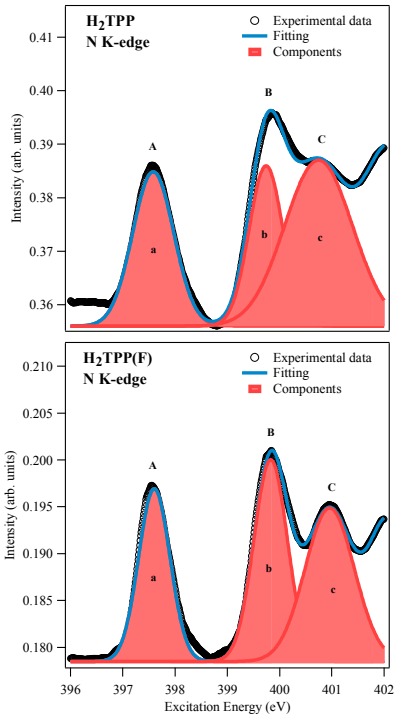

Fig. 8 Fitted [i] region of the N K-edge NEXAFS spectra of **H_2TPP (I)** (top) and **H_2TPP(F) (II)** (bottom).

The low number of possible *imo*s (four, see Table 1-ESI), the severe symmetry constraints and the consequent inherent simplicity of the N K-edge spectra make their preliminary assignment straightforward.[30,32]

Table 2. Excitation energy position (eV) of N K-edge transitions for **I** and **II** thick films. Δ*E* between similar features for **I** and **II** are also reported.

Component	I	Δ*E*	II	Δ*E*
a	397.57	-	397.60	-
b	399.74	2.17	399.83	2.23
c	400.75	3.18	400.96	3.36

As a matter of fact, the information pertaining to the relative positions of the N core levels (see Fig. 9, where experimental and calculated $1s^N$ spectra are compared)[8-9,48] and the unoccupied electronic structure of **I** and **II** (see Fig. 3) allows us to confidently ascribe the lower excitation energy region of **I** and **II** to 1s → $^{pmc}\pi_{\perp}$* transitions.

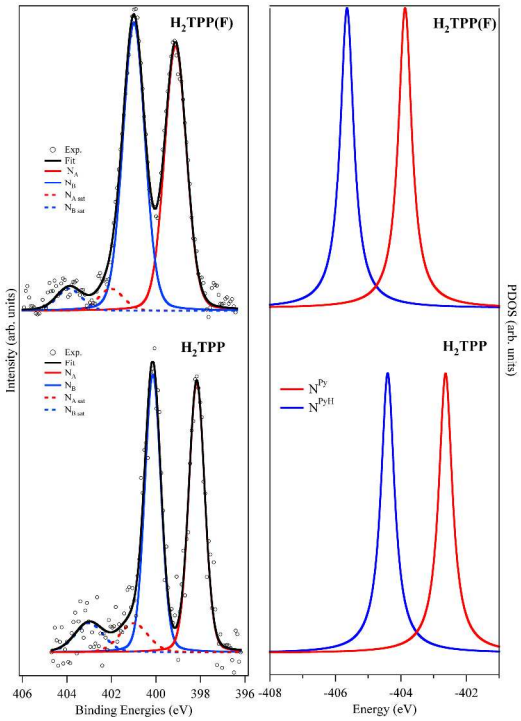

Fig. 9 (left panel) $1s^N$ core level spectra (background subtracted) from the **H2TPP (I)** and **H_2TPP(F) (II)** films. The single components, shown in the legend, are related to the different nitrogen chemical species of the two molecules.[8-9] (right panel) SR-ZORA DFT **H_2TPP (I)** and **H_2TPP(F) (II)** $1s^N$ PDOS.[8-9]

In particular, the lowest lying feature **A** has to be associated, both in **I** and **II**, to a single excitation event corresponding to the b_{1u} N^{Py}-based $1b_{3u}$ → $12b_{2g}$ transition in **I** and the $4b_{3u}$ → $21b_{2g}$ one in **II**. Similarly, a single excitation associated to the b_{1u} N^{PyH}-based $1b_{3u}$ → $12b_{2g}$ ($4b_{3u}$ → $21b_{2g}$) transition in **I** (**II**) is hidden under **B**. Qualitatively, the assignment of the feature **C** should include excitations associated to transitions whose *fmo*s lie necessarily beyond the feature **M** of Fig. 3.[30,32]

Before moving to the analysis of SR-ZORA TD-DFT results, both the unresponsiveness of the $^{pmc}\Pi_{\perp}$ subset (see Table 2) and the agreement of such an assignment with the angle-dependent linear dichroism characterizing the NEXAFS N K-edge

spectrum of a multilayer of **I**[17a] and the DFT transition potential results of Diller *et al.*[17b] deserve to be highlighted.

Qualitative predictions of the number of components in the experimental spectra perfectly fit the SR-ZORA TD-DFT results (see Tables 5-ESI and 6-ESI and Fig. 10). Nevertheless, the comparison of the N K-edge NEXAFS spectra (Fig. 8) with the $^{I}f^{N}$ and $^{II}f^{N}$ distributions of Fig. 10 testifies a really poor quantitative agreement between experimental evidences and theoretical data.

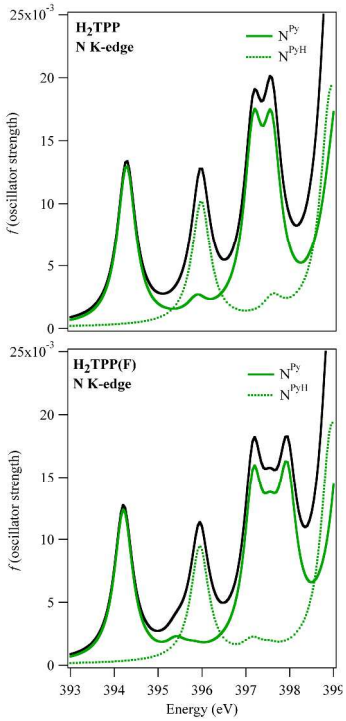

Fig. 10 SR-ZORA TD-DFT N 1s excitation spectra of **H_2TPP (I)** (top) and **H_2TPP(F) (II)** (bottom). Contributions from the different *imo*s are also displayed. Convoluted profiles have been obtained by using a Lorentzian broadening of 0.25 eV. SR-ZORA ionization limits may be deduced from the right panels of Fig. 9.[8-9]

In fact, besides the already revealed systematic excitation energy underestimation (in the present case ~2.5 eV),[25,13b] the relative position of the feature **^{t}B** (see Fig. 10) poorly reproduces the experimental outcomes for both **I** and **II**. In more detail, **^{t}A** and **^{t}B** features of Fig. 10 top and bottom are both due to a single excitation associated to the above indicated transitions. As far as **^{t}C** is concerned, its lower energy side is generated by one excitation associated to the $2a_g \rightarrow 15b_{1u}$ ($5a_g \rightarrow 24b_{1u}$) transition in **I** (**II**), while its higher *EE* side includes one (two) excitation(s) in **I** (**II**) (see Tables 5-ESI and 6-ESI). Incidentally, both the $15b_{1u}$ MO in **I** and the $24b_{1u}$ orbital in **II** correspond, as previously foreseen, to high lying $^{pmc}\pi_{\perp}$* levels with no nodes on N atoms (see 3D plots in Fig. 11), while lower lying $14b_{1u}$ and $23b_{1u}$ orbitals are e^{1}_{2u} Ph-based $\pi_{\parallel}$* levels.[32]

Moving to the analysis of $^{I}f^{N}$ and $^{II}f^{N}$ features, the comparison of experimental/theoretical excitation energy relative positions (ΔE(**b-a**)/ΔE(**^{t}B-^{t}A**) = 2.17/1.70 eV in **I** and 2.23/1.74 eV in **II**, ΔE(**c-a**)/ΔE(**^{t}C-^{t}A**) = 3.18/3.10 eV in **I** and 3.36/3.15 eV in **II**, see Tables 5-ESI, 6-ESI and Table 2)[49] states that the energy of the component **b** is underestimated by ~3.0 rather than ~2.5 eV as those of components **a** and **c**.[50]

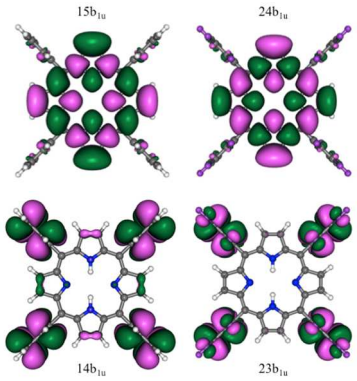

Fig. 11 3D plots of the $14b_{1u}$ and $15b_{1u}$ ($23b_{1u}$ and $24b_{1u}$) MOs of **H_2TPP (I)** (**H_2TPP(F) (II)**). Displayed isosurfaces correspond to ±0.01 $e^{1/2}Å^{3/2}$ values.

Such a failure of the adopted theoretical approach, even though herein particularly evident as a consequence of the very low number of expected and observed bands in the N K-edge spectra of **I** and **II**, is not particularly surprising. In fact, homogeneous theoretical results pertaining to the free phthalocyanine (H_2Pc)[11a,53] provided a ΔE between the lowest lying N^{Py}- and N^{PyH}-based 1s → $\pi_{\perp}$* transitions even smaller (1.55 eV) than the ΔEE(**^{t}B-^{t}A**) herein reported. The effect on the H_2Pc f^{N} distribution was less evident than in **I** and **II** as a consequence of the presence of the four meso N atoms, which concurred to increase the complexity of the H_2Pc NEXAFS spectrum. Moreover, it can be useful to remind that H_2Pc excitations associated to N^{m}-based 1s → $\pi_{\perp}$* transitions abut against the N^{PyH}-based ones (Fig. 17 of ref. 11a).

As a final consideration, it is noteworthy that, despite the above mentioned failure, SR-ZORA TD-DFT results perfectly reproduce the experimental unresponsiveness of the $^{pmc}\Pi_{\perp}$ subset, thus stressing the negligible perturbation induced by the Ph F decoration in the excitation energies of 1s → $^{pmc}\pi_{\perp}$* independently of the *imo*s localization.

F K-edge spectra. The [i] region of the F K-edge NEXAFS spectrum (see Fig. 12) consists of a single intense band centred at 688.51 eV.

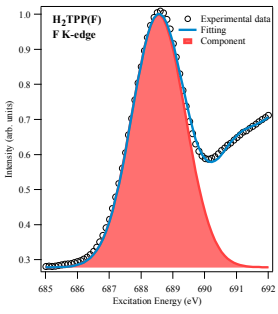

Fig. 12 Fitted [i] region of the fluorine K-edge NEXAFS spectra of **H_2TPP(F) (II)**.

The experimental information is surely rather poor, nevertheless the combined use of symmetry, orbitals and spectra appears to be once again the Hobson's choice to get some information from experimental evidences.

As reported in Table 1-ESI, the $F_{||}$-based linear combinations of 1s AOs correspond to the $1a_g + 1b_{1g} + 1b_{2u} + 1b_{3u}$ MOs, while those localized on $F_{\perp}$ span all the eight IRs of the D_{2h} point group. Although the number of F 1s-based MOs is quite large (20), they are closely spaced and the energy range they cover is quite narrow (see Fig. 13).[8]

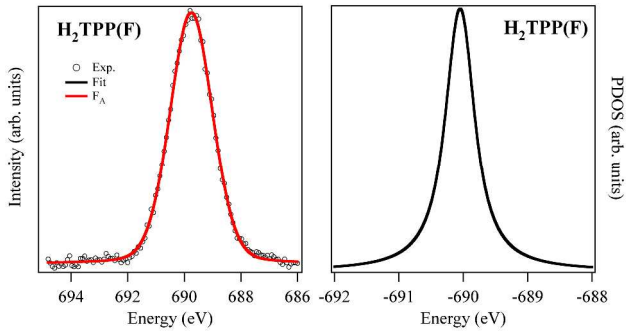

Fig. 13 (left panel) $1s^F$ core level spectra (background subtracted) from **H_2TPP(F) (II)** film.[8] (right panel) SR-ZORA DFT **H_2TPP(F) (II)** $1s^F$ PDOS.

Excitation energies and *f* values for the F 1s excitation spectrum as obtained from SR-ZORA TD-DFT[24] calculations are reported in Table 7-ESI, while the corresponding f^F distribution in the range 680 - 683 eV is displayed in Fig. 14 with contributions of different symmetries rather than of different *imol*s. The agreement between experiment and theory is satisfactory (the absolute excitation energies are underestimated by ~7 eV).[25,13b]

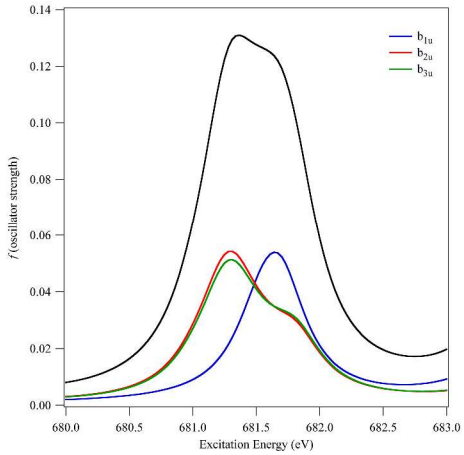

Fig. 14 SR-ZORA TD-DFT F 1s excitation spectrum **H_2TPP(F) (II)**. Contributions from the different symmetry are also displayed. Convoluted profiles have been obtained by using a Lorentzian broadening of 0.25 eV. SR-ZORA ionization limits may be deduced from the right panel of Fig. 13. [8]

Moreover, consistently with the inversed linear dichroism in F K-edge NEXAFS data recently published by de Oteyza *et al.* for fluorinated planar aromatic molecules,[54] SR-ZORA TD-DFT outcomes indicate that F-based b_{2u} and b_{3u} 1s → $\pi_{||}$* and b_{1u} 1s → σ* transitions share the same energy region (see Fig. 14). In more detail, the quite broad band reported in Fig. 12 includes excitations associated to transitions having the $\pi_{||}$* and σ* orbitals contributing to the feature **M** of Fig. 3 as *fmo*s.[32] Interestingly, no transition having linear combinations of the Ph-based e^2_{2u} MOs as *fmo*s and $f^F \geq 10 \times 10^{-3}$ is present in the energy range taken into account in Fig. 14.

Conclusions

Unoccupied states of two π-conjugated molecules, the tetrakis (phenyl)- and tetrakis(pentafluorophenyl)-porphyrin, have been thoroughly investigated by means of NEXAFS spectroscopy at the C, N and F K-edges. According to a well established procedure, the rationalization of experimental results collected from thin films of both molecules has been successfully guided by the outcomes of calculations carried out for isolated species in the framework of TD-DFT. Besides shedding new light on literature experimental results,[17a] theoretical outcomes herein reported provide valuable information about perturbations induced by the Ph fluorination on the unoccupied electronic structure of the pristine porphyrin macrocycle. The most evident, and rather unexpected, result is the *electronic inertness* of $^{pmc}\Pi_{\perp}$ transitions whose excitation energies, but not their *f* values, are substantially unaffected upon fluorination. Differently, $\Pi_{||}$ and, to a minor extent, $^{Ph}\Pi_{\perp}$ transitions undergo the expected blue shift when moving from **I** to **II**. Results herein reported complement those we published in the near past about the occupied electronic structure of **I** and **II**, thus providing the missing tile to get a thorough description of the halide decoration effects on the occupied and unoccupied electronic structure of title species, a necessary condition to address the electronic properties of their transition metal complexes.

The intrinsic simplicity of the N K-edge spectra of **I** and **II**, ultimately due to the presence of only two types of non-equivalent nitrogen atoms, revealed a sort of inappropriateness of the adopted theoretical method to quantitatively reproduce the energy difference between the lowest lying N-based 1s → $\pi_{\perp}$* transitions. Further investigations are needed to clarify this point.

Acknowledgements

Italian Ministry of the University and Research (PRIN-2010BNZ3F2, project DESCARTES), University of Padova (CPDA134272/13, project S_3MArTA), Computational Chemistry Community (C_3P) of the University of Padova are kindly acknowledged.

Notes and references

[a]*Institute for Physics, Supramolecular Systems Division "SMS", Humboldt Universitat zu Berlin, Brook-Taylor-Straße 6, 12489 Berlin, Germany. Fax: +49 30 2093 7443; Tel: ++49 30 2093 7716; E-mail: marco.nardi@physik.hu-berlin.de*

[b]*Istituto dei Materiali per l'Elettronica ed il Magnetismo, IMEM-CNR, Sezione di Trento, Via alla Cascata 56/C – Povo, 38100 Trento, Italy. E-mail: roberto.verucchi@cnr.it*

[c]*Dipartimento di Ingegneria "Enzo Ferrari", Università degli Studi di Modena e Reggio Emilia, Strada Vignolese 905, 41125 Modena, Italy; E-mail: luca.pasquali@unimore.it.*
[d]*TASC-INFM, MM building in Area Science Park, s.s.14 km 163.5, 34012Basovizza (Trieste) Italy. E-mail: angelo.giglia@ELETTRAdomain.*
[e]*Dipartimento di Scienze Chimiche e Farmaceutiche, Università di Trieste, Via L. Giogieri 1, 34127 Trieste, Italy. E-mail: fronzoni@units.it*
[f]*Dipartimento di Scienze Chimiche, Università degli Studi di Padova, Via Marzolo 1, 35131 Padova, Italy. Fax: +39 049 8275161; Tel: +39 049 8275164; E-mail: maurizio.casarin@unipd.it*
[g]*Istituto di Scienze e Tecnologie Molecolari del CNR, Via Marzolo 1, 35131 Padova, Italy*

Electronic Supplementary Information (ESI) available: Energy-ordered linear combinations of heavy atoms 1s AOs; Γ_{XS} representation products corresponding to electric dipole allowed transitions in D_{2h} symmetry Excitation energies and oscillator strengths *f* for the C and N (C, N and F) 1s excitation spectrum of **I** (**II**) from SR-ZORA TD-DFT calculations. See DOI: 10.1039/b000000x/

1 The Porphyrin Handbook, ed. K. M. Kadish, K. M. Smith, R. Guilard, Academic Press, New York, 2000.
2 D. Dini and M. Hanack, *J. Porphyr. Phthalocya.*, 2004, **8**, 915.
3 C. Di Natale, D. Monti and R. Paolesse, *Mater. Today*, 2010, **13**, 37.
4 A. Tsuda and A. Osuka, *Science*, 2001, **293**, 79.
5 M. Planells, A. Forneli, E. Martínez-Ferrero, A. Sánchez-Díaz, M. A. Sarmentero, P. Ballester, E. Palomares and B. C. O'Regan, *Appl. Phys. Lett.*, 2008, **92**, 153506.
6 A. P. Castano, P. Mroz and M. R. Hamblin, *Nature Rev. Canc.*, 2006, **6**, 535.
7 N. A. Rakow and K. S. Suslick, *Nature*, 2000, **406**, 710.
8 M. Nardi, R. Verucchi, L. Aversa, M. Casarin, A. Vittadini, N. Mahne, A. Giglia, S. Nannarone and S. Iannotta, *New J. Chem.*, 2013, **37**, 1036.
9 M. Nardi, R. Verucchi, C. Corradi, M. Pola, M. Casarin, A. Vittadini and S. Iannotta, *Phys. Chem. Chem. Phys.,* 2010, **12**, 871.
10 A detailed description of the supersonic molecular beam deposition approach can be found in refs. 8 and 9.
11 (a) M. V. Nardi, F. Detto, L. Aversa, R. Verucchi, G. Salviati, S. Iannotta and M. Casarin, *Phys. Chem. Chem. Phys.,* 2013, **15**, 12864; (b) G. Mangione, M. Sambi, M. V. Nardi and M. Casarin *Phys. Chem. Chem. Phys.,* 2014, **16**, 19852.
12 Amsterdam Density Functional version 2013.01. http://www.scm.com.
13 (a) M. Stener, G. Fronzoni and M. de Simone, *Chem. Phys. Lett.*, 2003, **373**, 115; (b) M. Casarin, P. Finetti, A. Vittadini, F. Wang and T. Ziegler, *J. Phys. Chem. A*, 2007, **111**, 5270.
14 E. K. U. Gross and W. Kohn, *Adv. Quantum Chem.*, 1990, **21**, 255.
15 R. van Leeuwen and E. J. Baerends, *Phys. Rev. A: At., Mol.,Opt. Phys.*, 1994, **49**, 2421.
16 J. H. van Lenthe, S. Faas and J. G. Snijders, *Chem. Phys. Lett.*, 2000, **328**, 107.
17 (a) G. Di Santo, C. Castellarin-Cudia, M. Fanetti, B. Taleatu, P. Borghetti, L. Sangaletti, L. Floreano, E. Magnano, F. Bondino and A. Goldoni, *J. Phys. Chem. C*, 2011, **115**, 4155; (b) K. Diller, F. Klappenberger, M. Marschall, K. Hermann, A. Nefedov, Ch. Wöll and J. V. Barth, *J. Chem. Phys.*, 2012, **136**, 014705.
18 S. Narioka, H. Ishii,Y. Ouchi, T. Yokoyama, T. Ohta and K. Seki, *J. Phys. Chem.*, 1995, **99**, 1332.
19 (a) L. Pasquali, A. De Luisa and S. Nannarone, *AIP Conf. Proc.*, 2004, **705**, 1142; (b) S. Nannarone, F. Borgatti, A. De Luisa, B. P. Doyle, G. C. Gazzadi, A. Giglia, P. Finetti, N. Mahne, L. Pasquali, M. Pedio, G. Selvaggi, G. Naletto, M. G. Pelizzo and G. Tondello, *AIP Conf. Proc.*, 2004, **705**, 450; (c) S. Nannarone, A. Giglia, N. Mahne, A. De Luisa, B. Doyle, F. Borgatti, M. Pedio, L. Pasquali, G. Naletto, M. G. Pelizzo and G. Tondello, *Notiz. Neutr. Luce Sincr.*, 2007, **12**, 8.
20 (a) E. Van Lenthe, E. J. Baerends and J. G. Snijders, *J. Chem. Phys.*, 1993, **99**, 4597; (b) E. Van Lenthe, E. J. Baerends and J. G. Snijders, *J. Chem. Phys.*, 1994, **101**, 9783; (c) E. Van Lenthe, A. W. Ehlers, E. J. Baerends and J. G. Snijders, *J. Chem. Phys.*, 1999, **110**, 8543.
21 E. van Lenthe and E. J. Baerends, *J. Comput. Chem.*, 2003, **24**, 1142.
22 G. L. Miessler, P. J. Fischer and D. A. Tarr, *Inorganic Chemistry*, 5th edition, Pearson: New York, 2013, p. 137.
23 R. S. Mulliken, *J. Chem. Phys.*, 1955, **23**, 1833.
24 F. Wang, T. Ziegler, E. van Lenthe, S. van Gisbergen and E. J. Baerends, *J. Chem. Phys.*, 2005, **122**, 204103, and references therein.
25 G. Fronzoni, M. Stener, P. Decleva, F. Wang, T. Ziegler, E. van Lenthe and E. J. Baerends, *Chem. Phys. Lett.*, 2005, **416**, 56.
26 It is well known[25] that this kind of functions is needed to properly describe transitions toward Rydberg states.
27 G. P. Moss, *Pure & Appl. Chem.*, 1987, **59**, 779.
28 (a) E. Hückel, *Z. Phys.*, 1931, **70**, 204; (b) E. Hückel, *Z. Phys.*, 1931, **72**, 310; (c) E. Hückel, *Z. Phys.*, 1932, **76**, 628.
29 The energy-ordered linear combinations of heavy atoms 1s AOs are collected in Table 1 of the electronic supplementary information (Table 1-ESI).
30 *pmc* unoccupied π* frontier orbitals[22] transform as $b_{2g} + b_{3g} + a_u + b_{1u}$. The low-lying $\pi_\perp$* MOs are: the $12b_{2g}$, $12b_{3g}$ and $11a_u$ MOs in **I** ($21b_{2g}$, $21b_{3g}$ and $20a_u$ MOs in **II**), all of them characterized by a quite homogeneous localization on *pmc* atoms (see Fig. 4). Besides the σ_h nodal plane, common to all of them, i) b_{2g} orbitals are anti-symmetric with respect to the σ_{yz} symmetry plane; namely, they have a nodal plane ⊥ to σ_h and passing through N^{PyH}; ii) b_{3g} orbitals are anti-symmetric with respect to the σ_{xz} symmetry plane; namely, they have a nodal plane ⊥ to σ_h and passing though N^{Py}; iii) a_u orbitals are anti-symmetric with respect to both σ_{xz} and σ_{yz} symmetry planes; namely, they have two nodal planes ⊥ to σ_h, the former passing through N^{Py}, the latter through N^{PyH}; iv) b_{1u} orbitals are symmetric with respect to both σ_{xz} and σ_{yz} symmetry planes.[31] Nodal properties of π* frontier orbitals have been here emphasized because they can be helpfully exploited to qualitatively foresee the localization of 1s → π* electric dipole allowed transitions.
31 (a) M. Orchin and H. H. Jaffé, *Symmetry, Orbitals, and Spectra (S.O.S.)*, Wiley-Interscience: New York, 1971; (b) B. E. Douglas and C. A. Hollingsworth, *Symmetry in Bonding and Spectra*, Academic Press: New York, 1985.
32 The MOs of **I** contributing to **M** in Fig. 3 are the $11a_u + 33a_g + 30b_{2u} + 30b_{3u} + 14b_{1u} + 27b_{1g} + 12a_u + 13\ b_{2g} + 13b_{3g}$ ones. With the exclusion of the $\pi_\perp$* $11a_u$ MO (see Fig. 4), the remaining eight orbitals correspond to the linear combinations of the Ph-based e_{2u} $\pi_\parallel$* levels. Among them, the $12a_u$, $13b_{2g}$, $13b_{3g}$, $14b_{1u}$ MOs are the e_{2u}-like $\pi_\parallel$* partners with a node on the C^{25} and C^{45} atoms (hereafter, e^1_{2u}). The MOs of **II** contributing to **M** in Fig. 3 are the $20a_u + 44a_g + 41b_{3u} + 41b_{2u} + 38b_{1g} + 23b_{1u} + 21a_u$

+ $22b_{2g}$ + $22b_{3g}$ + $45a_g$ + $42b_{2u}$ + $42b_{3u}$ + $39b_{1g}$ ones. Similarly to **I**, the $\pi_\perp$* $20a_u$ MO is localized on the *pmc* atoms, while the following eight orbitals correspond to the linear combinations of the Ph-based e_{2u} $\pi_\parallel$* levels, antibonding in nature with respect to the C–F π interaction. Moreover, the $21a_u$ + $22b_{2g}$ + $22b_{3g}$ + $23b_{1u}$ MOs are the e^1_{2u}-like $\pi_\parallel$* partners with a node on the C^{25}, C^{45} and F^{65} atoms. As far as the last four orbitals ($45a_g$ + $42b_{2u}$ + $42b_{3u}$ + $39b_{1g}$ MOs) are concerned, they have a C–F σ* character. Both in **I** and **II**, a huge number of closely spaced π* and σ* MOs is present beyond **M**. Their detailed list is useless and is not herein reported due to space reasons.

33 R. De Francesco, M. Stener and G. Fronzoni, *J. Phys Chem. A*, 2012, **116**, 2885.

34 M. Linares, S. Stafstrom and P. Norman, *J. Chem. Phys.*, 2009, **130**, 104305.

35 V. Yu. Aristov, O. V. Molodtsova, V. Maslyuk, D. V. Vyalikh, V. M. Zhilin, Yu. A. Ossipyan, T. Bredowe, I. Mertig and M. Knupfer, *Appl. Surf. Sci.*, 2007, **254**, 20.

36 Γ_{XS} representation products corresponding to the electric dipole allowed transitions in the D_{2h} symmetry are summarized in Table 2-ESI.

37 The NEXAFS spectrum of **I** at the C K-edge perfectly matches the one recently published by some of us for *trans*-$TPP(NH_2)_2$.[38]

38 A. Basagni, L. Colazzo, F. Sedona, M. Di Marino, T. Carofiglio, E. Lubian, D. Forrer, A. Vittadini, M. Casarin, A. Verdini, A. Cossaro, L. Floreano and M. Sambi, *Chem.-Eur. J.*, 2014, **20**, 14296.

39 NEXAFS spectra reported in Fig. 6 extends for ~5 eV (see also Table 1). The selected *fmo* number allowed us to cover an excitation energy range of ~8 eV.

40 The angle-dependent linear dichroism in the NEXAFS C K-edge spectrum of a multilayer of **I** is characterized by the disappearance of the lowest lying **S** + **A** band envelope when switching from the light polarization $\perp$ to *pmc* (θ = 90°, p-polarization), to the light polarization $\parallel$ to *pmc* (θ = 0°, s-polarization).[17] Accordingly, Di Santo *et al.*[17a] assigned the **S** + **A** band envelope to $\Pi_\perp$ transitions, without entering in more detail. Moreover, consistently with the *quasi* $\perp$ orientation of Ph rings with respect to *pmc* in the isolated **I**, they found that the intense peak due to the Ph-based 1s ➞ π* transitions in p-polarization still dominates the NEXAFS spectrum recorded in s-polarization.

41 Among the excitations 8 – 19, the 12 – 19 ones correspond to $\Pi_\parallel$ transitions with the highest $^{\mathbf{I}}f^{\mathbf{C}}$ values.

42 The six π orbitals of an isolated Ph ring transform, in the D_{6h} symmetry, as: a_{2u} + e^1_{1g} + e^2_{1g} + e^1_{2u} + e^2_{2u} + b_{2g}. The first (second) three are occupied (unoccupied).[31]

43 Excitations selected as internal gauge imply the following correlations: $1^{\mathbf{I}} \leftrightarrow 1^{\mathbf{II}}$, $3^{\mathbf{I}} \leftrightarrow 4^{\mathbf{II}}$, $4^{\mathbf{I}} \leftrightarrow 3^{\mathbf{II}}$, $5^{\mathbf{I}} \leftrightarrow 5^{\mathbf{II}}$, $6^{\mathbf{I}} \leftrightarrow 6^{\mathbf{II}}$, $9^{\mathbf{I}} \leftrightarrow 8^{\mathbf{II}}$.

44 The huge blue shift of the $\Pi_\parallel$ set involves transitions localized on fluorinated C^{Ph} atoms. Excitation energies corresponding to transitions whose *imo*s are C^{25}-based 1s AOs are scarcely affected.

45 The increase of *f* values upon fluorination is ultimately due to the rise of an order of magnitude of the corresponding *z* contributions to the transition dipole moments. Irrespective of their low *f* values, both C^2-based $8b_{3u}$ ➞ $12b_{2g}^{(100)}$ and $7b_{1g}$ ➞ $11a_u^{(100)}$ transitions belong to the $^{pmc}\Pi_\perp$ subset.

46 The $13a_u$ ($23a_u$) MO is the third (fourth) unoccupied level of a_u symmetry in **I** (**II**). The comparison between the 3D plots, not herein reported, of the $22a_u$ and $23a_u$ MOs of **II** revealed the σ* nature of the former and the $\pi_\perp$* character of the latter.

47 Upon fluorination, C^{Py}- and C^m-based 1s AOs are blue shifted by ~1.25 eV and 1.60 eV, respectively. The shift toward higher binding energies is much more pronounced for C^{Ph}-based 1s AOs: 2.5 and 4.3 eV for non-fluorinated and fluorinated C atoms, respectively. Blue shifts of $^{pmc}\pi_\perp$* and $^{Ph}\pi_\parallel$* levels are 0.9 and 0.7 eV, respectively.

48 The experimental (theoretical) ΔE between N^{Py} and N^{PyH} 1s-based levels is 1.90 (1.73) eV both in $\mathbf{I}^9$ and **II**.[8] Upon fluorination, N^{Py}- and N^{PyH}-based 1s AOs are both blue shifted by 0.80 eV,[8-9] while $^{pmc}\pi_\perp$* levels are downshifted by 0.9 eV.[47]

49 The **C** excitation energy has been estimated, for both **I** and **II**, as the mean energy values between the 3rd and 4th excitation energies (Tables 5-ESI and 6-ESI).

50 A further series of numerical experiments, carried out either by reducing the D_{2h} symmetry through the *pmc* tilting, or by using an exchange correlation potential (SAOP)[51] having the correct asymptotic behaviour but different from the LB94 functional did not improve the $^{\mathbf{t}}\mathbf{B}$ relative position.[52]

51 P. R. T. Schipper, O. V. Gritsenko, S. J. A. van Gisbergen and E. J. Baerends, *J. Chem. Phys.*, 2000, **112**, 1344.

52 Fronzoni *et al.* showed that both relative *EE*s and *f* are not very sensitive to the exchange correlation potential choice, provided the asymptotic behaviour is correct.[25]

53 The quasi degenerate H_2Pc $6b_{3g}$ and $6b_{2g}$ unoccupied frontier[22] orbitals have the same symmetry, localization and nodal properties[30] of the $12b_{3g}$ and $12b_{2g}$ ones in **I**.

54 D. G. de Oteyza, A. Sakko, A. El-Sayed, E. Goiri, L. Floreano, A. Cossaro, J. M. Garcia-Lastra, A. Rubio and J. E. Ortega, *Phys. Rev. B*, 2012, **86**, 075469.